

Numerical Heat Transfer, Part A: Applications



An International Journal of Computation and Methodology

ISSN: 1040-7782 (Print) 1521-0634 (Online) Journal homepage: http://www.tandfonline.com/loi/unht20

Combined parameter and state estimation in the radio frequency hyperthermia treatment of cancer

Leonardo Antonio Bermeo Varon, Helcio Rangel Barreto Orlande & Guillermo Enrique Eliçabe

To cite this article: Leonardo Antonio Bermeo Varon, Helcio Rangel Barreto Orlande & Guillermo Enrique Eliçabe (2016) Combined parameter and state estimation in the radio frequency hyperthermia treatment of cancer, Numerical Heat Transfer, Part A: Applications, 70:6, 581-594

To link to this article: http://dx.doi.org/10.1080/10407782.2016.1193342

	Published online: 18 Aug 2016.
	Submit your article to this journal 🗷
lılıl	Article views: 68
Q	View related articles 🗷
CrossMark	View Crossmark data 🗹
4	Citing articles: 1 View citing articles 🗹

Full Terms & Conditions of access and use can be found at http://www.tandfonline.com/action/journalInformation?journalCode=unht20



Combined parameter and state estimation in the radio frequency hyperthermia treatment of cancer

Leonardo Antonio Bermeo Varon^a, Helcio Rangel Barreto Orlande^a, and Guillermo Enrique Eliçabe^b

^aDepartment of Mechanical Engineering, Federal University of Rio de Janeiro – UFRJ, Rio de Janeiro, Brazil; ^bInstitute of Materials Science and Technology - INTEMA (CONICET), University of Mar del Plata, Mar del Plata, Argentina

ABSTRACT

Particle filters are general methods for the solution of state estimation problems, which can be applied to nonlinear models with non-Gaussian uncertainties. In this paper, an algorithm of the particle filter is used for the simultaneous estimation of model parameters and state variables in a bioheat transfer problem associated with the radio frequency (RF) hyperthermia treatment of cancer. Results obtained with simulated measurements indicate an excellent agreement between the estimated and the exact quantities, even for cases with large uncertainties in the measurements, as well as in the evolution and measurement models.

ARTICLE HISTORY

Received 27 January 2016 Accepted 20 April 2016

1. Introduction

Particle filter methods are used to solve inverse state estimation problems with sequential Bayesian inference. The application of such methods relies on the available measured data, as well as on stochastic mathematical models for the evolution of the dynamic state variables and for the measurements [1, 2]. Different particle filter methods have been developed in order to represent the posterior density of such variables in terms of random samples (particles) and associated weights. It is not intended to make a literature review of the available algorithms here, but to mention some that served as the basis for the algorithm used in this work. The sequential importance sampling (SIS) algorithm introduced in a study by Hammersley and Hanscomb [3] was lately modified to include a resampling step (sampling importance resampling - SIR algorithm) [4, 5]. The resampling step avoids the degeneration of particles, characterized by only few particles with large weights, and large computational work to advance particles with negligible weights. On the other hand, the SIR algorithm may suffer from sample impoverishment that is characterized by many identical particles and the auxiliary particle filter (APF) was developed to avoid such deleterious effect [6]. In the APF, resampling is applied over the particles at the previous time instant, by using the measurements at the current time instant. For the simultaneous estimation of model parameters and state variables with the aforementioned algorithms, evolution models for the parameters need to be specified; although a general random walk model can be applied, it might fast degenerate the particles. As a result, algorithms for the simultaneous estimation of parameters and state variables have been developed, like that of Liu and West [7], which is used in this work. In Liu and West's algorithm, the parameters are represented as a mixture of Gaussian kernels [7, 8].

The particle filter methods have been recently applied to different biomedical applications, including the hyperthermia treatment of cancer [9–16]. Hyperthermia is a cancer treatment where the tumor temperatures are raised to values typically between 40°C and 45°C, with heating imposed

	Nomenc	lature	
c_p	specific heat	Greeks	
Ď	number of measurements	δ	discount factor for Liu & West's algorithm
E	electric field strength	ε	permittivity
f	frequency	$\pi(a b)$	conditional probability of a when b is given
f, h	general functions for the evolution and	ρ	density
	observation models, respectively	Ω	surface of the domain
H	intensity of the magnetic field	Ω'_1, Ω'_2	boundary patches with electrodes set to
h_f	heat transfer coefficient		voltages U and ground, respectively
k [']	thermal conductivity	ω_b	blood perfusion rate
L_x , L_y , L_z	domain dimensions in the x , y , and	φ	electric potential
	z directions, respectively	θ	parameter vector
n	measurement noise vector	Θ	volumetric concentration of
n	number of nanoparticles		nanoparticles
N	number of particles for the particle filter	σ	electric conductivity
m	Gaussian kernel center	χ	susceptibility of the magnetic nanoparticles
M	total number of elements	μ_0	dielectric permeability constant
Q	volumetric heat source	ν	constant standard deviation
r	mean radius of nanoparticles	ξ	Gaussian random vector with zero mean and
R	radius of the tumor		constant standard deviation
S	interface between the tumor and the		
	surrounding tissue	Superscri	pts
T	temperature	i	particle index
T_b	blood temperature	meas	measurements
T_f	temperature of the surrounding medium		
ť	time	Subscript	's
U	voltage	1	health tissue
w	weights of the particles	2	tumor
X	state vector	3	nanoparticles
x,y,z	Cartesian coordinates	b	blood
v	state noise vector	e	electrical
V	Monte Carlo covariance matrix of the posterior	est	estimated
	distribution	exa	exact
V	volume	k	index to time step
z	vector of measurements	m	metabolism

by electromagnetic waves [17-51]. This treatment aims either at directly killing the cancer cells or making them more susceptible to the effects of radiotherapy [28] or chemotherapy [29]. Depending on several factors, including the type of the heat source, geometry, and tumor location, healthy tissues can be overly heated and thermally damaged as well. With the recent advancement of nanotechnology, nanoparticles have been loaded inside the tumor, in order to locally increase the absorption of the electromagnetic waves in the radiofrequency [15, 30-40] and near-infrared [16, 41-46] ranges. As a result, the tumor is imposed larger temperature increases than the surrounding healthy tissues [47–51].

In the present work, the analysis performed by the authors in reference [15] is extended to a threedimensional case, as well as to an inverse problem of simultaneous estimation of state variables and model parameters. The inverse problem is solved with simulated measurements for an idealized case in the hyperthermia treatment of cancer, imposed by electromagnetic waves in the radiofrequency range and by considering the tumor loaded with iron oxide nanoparticles (Fe₃O₄).

2. Parameter and state estimation problem

In the state estimation problem, consider a model for the evolution of the vector \mathbf{x} in the following form [52]:

$$\mathbf{x}_k = \mathbf{f}_k(\mathbf{x}_{k-1}, \mathbf{\theta}, \mathbf{v}_{k-1}) \tag{1}$$



where the subscript k = 1, 2, ..., denotes a time instant t_k in a dynamic problem. The vector $\mathbf{x} \in \mathbb{R}^{n_x}$ is called the state vector and contains the variables to be dynamically estimated. This vector advances in accordance with the state evolution model given by Equation (1), where \mathbf{f}_k is a general function of the state variables \mathbf{x} , of the vector of parameters θ and of the state noise vector $\mathbf{v} \in R^{n_v}$ [52, 53].

The measurements $\mathbf{z}_k \in \mathbb{R}^D$ are available at t_k , k = 1, 2, ..., and are related to the state variables \mathbf{x}_k through the observation model \mathbf{h}_k given by

$$\mathbf{z}_k = \mathbf{h}_k(\mathbf{x}_k, \mathbf{\theta}, \mathbf{n}_k) \tag{2}$$

where $\mathbf{n} \in \mathbb{R}^D$ is the measurement noise.

For the evolution-observation models given by Equations (1) and (2), the noise vectors are also assumed to be mutually independent and independent of the initial state $\mathbf{x}_0[2]$. Other hypotheses that apply to the evolution-observation models given by Equations (1) and (2) can be found in references [1-8, 52-54].

The filtering form of the state estimation problem is considered in this paper. By assuming that π $(\mathbf{x}_0 \mid \mathbf{z}_0, \mathbf{\theta}) = \pi(\mathbf{x}_0)$ is available at time t_0 , $\pi(\mathbf{x}_k \mid \mathbf{z}_{1:k}, \mathbf{\theta})$ is obtained with Bayesian filters in two sequential steps. The state evolution model is used to advance the vector of state variables from time t_{k-1} to time t_k in the prediction step, thus obtaining a prior distribution $\pi(\mathbf{x}_k)$ for the state variables at time t_k . The information provided by the measurements is then adjoined to this prior distribution in the update step through Bayes' theorem, by using the likelihood function $\pi(\mathbf{z}_k | \mathbf{x}_k, \mathbf{\theta})$ [1-8, 52-54].

The particle filter method is used in this paper due to the nonlinear character of the present state estimation problem. The particle filter method is a Monte Carlo technique, where the required posterior density function is represented by a set of random samples (particles) with associated weights; the statistics of the posterior distribution is computed based on these samples and weights [1-8, 52-54]. Let \mathbf{x}_k^i denote the particle i, with associated weight w_k^i , $i = 0, \dots, N$, at time t_k , where N is the number of particles. Also, let the set of all state variables up to t_k be denoted by $\mathbf{x}_{0:k} = \{\mathbf{x}_i,$ j=0, 1, ..., k. The weights are normalized so that $\sum_{i=1}^{N} w_k^i = 1$. Then, the posterior marginal distribution, can be approximated by [2, 53]:

$$\pi(\mathbf{x}_k \mid \mathbf{z}_k, \mathbf{0}) \approx \sum_{i=1}^N w_k^i \delta(\mathbf{x}_k - \mathbf{x}_k^i)$$
 (3)

with weights computed from [53]:

$$w_k^i \propto w_{k-1}^i \pi(\mathbf{z}_k \,|\, \mathbf{x}_k^i, \mathbf{\theta}) \tag{4}$$

Equations (3) and (4) can be applied recursively for the estimation of $\pi(\mathbf{x}_k | \mathbf{z}_k, \boldsymbol{\theta})$ at each time step, for θ deterministically known, such as in the SIR and ASIR algorithms. If these parameters are to be estimated simultaneously with the state variables, one possibility is to apply the SIR or ASIR filters by mimicking the parameters as state variables with an evolution model, for example, in the form of a random walk process. On the other hand, the simulation of parameters as state variables might fast degenerate the particles [7, 13]. The algorithm by Liu and West [7], which is based on the ASIR version of the particle filter, can be used for the estimation of the posterior probability distribution $\pi(\mathbf{x}_k, \mathbf{\theta} | \mathbf{z}_{1:k})$. Therefore, the particles need to be extended to $\{\mathbf{x}_k^i, \mathbf{\theta}_k^i : i = 0, \dots, N\}$. The subscript k for the parameters θ and associated quantities is used to indicate that they refer to the posterior distribution at time t_k ; it does not mean that such quantities are time dependent. The particle filter algorithm by Liu and West is based on the hypothesis that the vector of nondynamic parameters θ is represented by [8]

$$\pi(\mathbf{\theta}|\mathbf{z}_{1:k-1}) \approx \sum_{i=1}^{N} w_{k-1}^{i} N(\mathbf{\theta} \mid \mathbf{m}_{k-1}^{i}, h^{2} \mathbf{V}_{k-1})$$
 (5)

where $N(\theta | \mathbf{a}, \mathbf{B})$ is a multivariate Gaussian density with mean \mathbf{a} and covariance matrix \mathbf{B} , while h is a smoothing factor and V_{k-1} is the Monte Carlo posterior covariance matrix at time t_{k-1} . Equation (5) shows that the above density is a mixture of Gaussian distributions $N(\theta | \mathbf{m}_{k-1}^i, h^2 \mathbf{V}_{k-1})$ weighted by

Liu and West's algorithm [7].

```
Select a value for \delta \in [0.95; 0.99], then compute a with equation (7) and h^2 with equation (8).
   For i = 1, ..., N
   Compute \mathbf{m}_{k-1}^i with Equation (6) and calculate \mu_k^i = E[\mathbf{x}_k | \mathbf{x}_{k-1}^i, \mathbf{m}_{k-1}^i]. Use the likelihood density to calculate the corresponding
   weights w_k^i = \pi(\mathbf{z}_k | \mu_k^i, \mathbf{m}_{k-1}^i) w_{k-1}^i.
Calculate the total weight t = \sum_{i} w_{k}^{i};
   Normalize the particle weights, that is, for i = 1, ..., N let w_k^i = t^{-1}w_k^i.
Resample the particles as follows:
   Construct the cumulative sum of weights (CSW) by computing c_i = c_{i-1} + w_k^i for i = 1, ..., N with c_0 = 0.
   Let i = 1 and draw a starting point u_1 from the uniform distribution U[0,N^{-1}]
   For j = 1, ..., N
   Move along the CSW by making u_i = u_1 + N^{-1}(j-1)
   While u_i > u_i make i = i + 1
   Assign parent ij = i.
For j = 1, ..., N
   Draw samples \theta_k^j from N(\theta_k^j | \mathbf{m}_{k-1}^{ij}, h^2 \mathbf{V}_{k-1}), by using the parent ij.
   Draw particles \mathbf{x}_{k}^{j} from the prior density \pi(\mathbf{x}_{k}|\mathbf{x}_{k-1}^{ij},\mathbf{\theta}_{k}^{j}), by using the parent ij.
   Calculate the correspondent weights w_k^j = \frac{\pi(\mathbf{z}_k | \mathbf{x}_k^j, \mathbf{0}_k^j)}{\pi(\mathbf{z}_k | \mathbf{u}_k^j, \mathbf{m}_k^j)}
Calculate the total weight t = \sum_i w_k^i;
Normalize the particle weights, that is, for i = 1, ..., N let w_k^i = t^{-1}w_k^i.
```

the sample weights w_{k-1}^i . The Gaussian kernel centers \mathbf{m}_{k-1}^i are specified by using the shrinkage rule[8]:

$$\mathbf{m}_{k-1}^{i} = a\,\mathbf{\theta}_{k-1}^{i} + (1-a)\overline{\mathbf{\theta}}_{k-1} \tag{6}$$

where $\overline{\theta}_{k-1}$ is the mean of θ at time t_{k-1} . The shrinkage factor a is computed by

$$a = \frac{3\delta - 1}{2\delta} \tag{7}$$

where $0.95 < \delta < 0.99$ is a discount factor. The smoothing factor, h, also depends on the shrinkage factor, as follows

$$h^2 = 1 - a^2 (8)$$

The algorithm by Liu and West used in this work is summarized in Table 1.

By assuming that the measurement errors are additive, uncorrelated, Gaussian random variables with zero means and known constant standard deviation, v, and independent of the state variables, the likelihood function for each particle \mathbf{x}_k^i is then expressed as [2, 52, 53]:

$$\pi(\mathbf{z}_{k}^{meas}|\mathbf{x}_{k}^{i},\boldsymbol{\theta}) = (2\pi)^{-D/2}\nu^{-D}\exp\left\{-\frac{1}{2}\frac{\left[\mathbf{z}_{k}^{meas} - \mathbf{z}_{k}(\mathbf{x}_{k}^{i},\boldsymbol{\theta})\right]^{T}\left[\mathbf{z}_{k}^{meas} - \mathbf{z}_{k}(\mathbf{x}_{k}^{i},\boldsymbol{\theta})\right]}{\nu^{2}}\right\}$$
(9)

where $\mathbf{z}_k(\mathbf{x}_k^i, \mathbf{\theta})$ is obtained from the observation model given by equation (2) and D is the number of measurements.

3. Radiofrequency hyperthermia using iron oxide nanoparticles

Radiofrequency hyperthermia therapy is a cancer treatment for partial or total elimination of a solid tumor through the heating imposed by induction of electromagnetic waves in the range from 0.1 MHz to 100 MHz [18-24]. The temperature levels reached by the tumor cells might be sufficient for their destruction or to make them more susceptible to the effects of radiation or chemotherapy drugs [28, 29, 55, 56]. Currently, the combination of radiofrequency hyperthermia with tissues loaded with nanoparticles has been of great interest. In this kind of therapy, nanoparticles introduced into the tumor locally increase the absorption of the imposed electromagnetic waves, so that its temperature increases at a rate higher than that in the healthy surrounding tissues that do not contain nanoparticles. Therefore, thermal damage is imposed to the tumor without significantly affecting the healthy tissues [15, 30-40].

In the study of radiofrequency hyperthermia, the mathematical formulation of the physical problem involves Maxwell's equations with frequency-dependent properties and a bioheat transfer model [57]. The solution of the mathematical formulation requires the knowledge of several thermophysical properties and other input parameters, which are not widely known and exhibit variability from individual to individual, or even for the same individual under different physiological conditions. Therefore, the numerical simulation of the problem related to hyperthermia needs to be performed under the effects of large uncertainty. On the other hand, recent technological advancements permit the temperature measurement of the tissues of the body, such as through the magnetic resonance technique [58]. If such measurements are available, the numerical simulation of the radiofrequency problem containing uncertainties can be performed as a state estimation problem [5]. In the approach considered here, the radiofrequency hyperthermia problem is treated as an inverse problem of parameter and state estimation, with minimally invasive measurements. The focus of this work is the accurate prediction of the temperature field in tumor and healthy tissues, where iron oxide nanoparticles (Fe₃O₄) are loaded in the tumor region in order to enhance this cancer treatment and reduce damages to the healthy cells.

3.1. Mathematical formulation

The physical problem considered in this work involves a three-dimensional domain, consisting of a parallelepiped (healthy biological tissue) Ω_1 , with a spherical inclusion (tumor) Ω_2 , as shown by Figure 1. Heating is imposed by RF waves through the electrodes Ω'_1 and Ω'_2 . Heat generated by RF waves inside the domain is propagated by conduction and blood perfusion. The electric potential within the domain can be obtained by solving the following Laplace's equation [59]:

$$\nabla \cdot [\varepsilon(x, y, z) \nabla \varphi(x, y, z)] = 0 \quad x, y, z \in \Omega_1 \cup \Omega_2$$
 (10)

where φ is the potential, (x,y,z) are the Cartesian coordinates, and ε is the permittivity, which varies spatially depending on the tissue and tumor regions. The interface between the tumor and normal

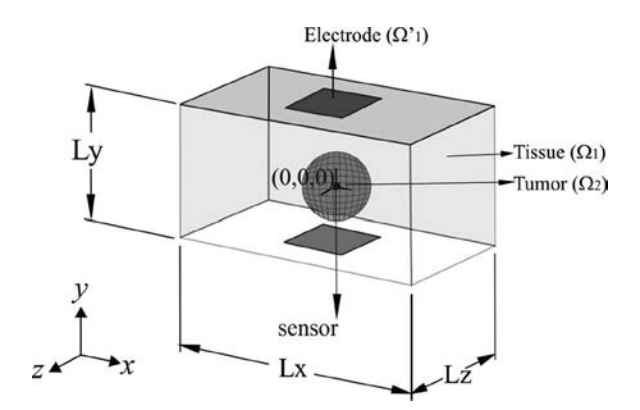


Figure 1. Geometry.

tissues is assumed to have ideal electric contact. The boundary conditions for the electrical problem are given by

$$\varphi(x, y, z) = U \text{ at } \Omega_1' \tag{11}$$

$$\varphi(x, y, z) = 0 \text{ at } \Omega_2' \tag{12}$$

$$\nabla \varphi(x, y, z) \cdot \mathbf{n} = 0 \text{ elsewhere over the boundary}$$
 (13)

where U denotes the imposed electric potential with respect to ground.

After computing the electric potential, one can calculate the electric field strength, E, and the intensity of the magnetic field, H, respectively, by

$$\mathbf{E}(x, y, z) = -\nabla \varphi(x, y, z) \tag{14}$$

$$|\mathbf{H}(x, y, z)| = \frac{1}{1 + N(\chi)} \frac{|\mathbf{E}(x, y, z)|}{\mu_0 \pi f R}$$
 (15)

where $N(\chi) = 1/3$ is the demagnetizing factor of the composite tissue [31, 36], χ is the susceptibility of the magnetic nanoparticles that can be described as the complex number $\chi = \chi' + i\chi''$ [60, 61], μ_0 is the dielectric constant permeability of free space ($\mu_0 = 4\pi \times 10^{-7}$ T m A⁻¹), f is the electromagnetic frequency, and R is the radius of magnetic induction loop.

The heat source in the healthy tissue Ω_1 , which does not contain nanoparticles, is given by

$$Q_{e_1}(x, y, z) = \frac{\sigma_1 |\mathbf{E}(x, y, z)|^2}{2}$$
 (16)

where σ_1 is the electric conductivity of the tissue.

Nanoparticles are supposed to be ideally located only within the tumor. The heat source in the tumor, due to induction of magnetic nanoparticles by electromagnetic effects as well as by electrical current, can be calculated by [36]

$$Q_{e_2}(x, y, z) = (1 - \mathbf{\Theta}) \frac{\sigma_2 |\mathbf{E}(x, y, z)|^2}{2} + \mathbf{\Theta} \left[\frac{9}{16} \frac{\chi''}{\mu_0 \pi f R^2} |\mathbf{E}(x, y, z)|^2 \right]$$
(17)

where $\mathbf{\Theta} = 4n\pi r^3/3V$ is the volumetric concentration of nanoparticles, r is the mean radius of the supposedly spherical nanoparticles, n is the number of nanoparticles, V is the volume of the tumor, and σ_2 is the electrical conductivity of the tumor tissue embedded with nanoparticles, which can be approximated by a mixture of the two materials, that is, $1/\sigma_2 = (1-\mathbf{\Theta})/\sigma_2' + \mathbf{\Theta}/\sigma_3$ where σ_2' and σ_3 are the electrical conductivity of tumor and nanoparticles, respectively [30]. The permittivity of the tumor tissue embedded with nanoparticles is approximated by the permittivity of the tumor, because the concentration of nanoparticles is too small and differences in this parameter for biological tissues and nanoparticles are not large [31].

The mathematical formulation for bioheat transfer in this work is described by Pennes's equation [57], that is

$$\rho(x, y, z)c_p(x, y, z)\frac{\partial T(x, y, z, t)}{\partial t} = \nabla \cdot [k(x, y, z)\nabla T(x, y, z, t)] + Q(x, y, z, t)$$
(18)

where ρ is the density, c_p is the specific heat, T is the temperature, k is the thermal conductivity, and Q is the heat source per unit volume given by

$$Q(x, y, z, t) = \rho_b c_{p,b} \omega_b(x, y, z) [T_b - T(x, y, z, t)] + Q_m(x, y, z) + Q_e(x, y, z)$$
(19)

where ω_b is the blood perfusion rate, ρ_b is the blood density, $c_{p,b}$ is the specific heat of blood, T_b is the blood temperature, Q_m is the metabolic heat source, and Q_e is the electrical heat source generated by radiofrequency external excitation given by equation (16) or (17). The tumor and



normal tissues are assumed to be in ideal thermal contact. The thermal boundary conditions are given by

$$k_{1} \frac{\partial T}{\partial x} = 0 \qquad \text{at } x = -\frac{L_{x}}{2} \text{ and } x = +\frac{L_{x}}{2}, -\frac{L_{y}}{2} < y < +\frac{L_{y}}{2}, \\ -\frac{L_{z}}{2} < z < +\frac{L_{z}}{2} \\ k_{1} \frac{\partial T}{\partial z} = 0 \qquad \text{at } z = -\frac{L_{z}}{2} \text{ and } z = +\frac{L_{z}}{2}, -\frac{L_{x}}{2} < x < +\frac{L_{x}}{2}, \\ -\frac{L_{y}}{2} < y < +\frac{L_{y}}{2} \\ -k_{1} \frac{\partial T}{\partial y} + h_{f}T = h_{f}T_{f} \qquad \text{at } y = -\frac{L_{y}}{2}, -\frac{L_{x}}{2} < x < +\frac{L_{x}}{2}, -\frac{L_{z}}{2} < z < +\frac{L_{z}}{2} \\ k_{1} \frac{\partial T}{\partial y} + h_{f}T = h_{f}T_{f} \qquad \text{at } y = +\frac{L_{y}}{2}, -\frac{L_{x}}{2} < x < +\frac{L_{x}}{2}, -\frac{L_{z}}{2} < z < +\frac{L_{z}}{2} \end{cases}$$

$$(20)$$

where h_f is the heat transfer coefficient; T_f is the temperature of the surrounding medium; L_x , L_y , and L_z are the domain lengths in the x, y, and z directions, respectively. The region is supposed to be initially at the steady-state temperature of the problem, when the electric heat source imposed by the radiofrequency external excitation is null.

The solution of the forward problem was obtained with finite elements by using COMSOL Multiphysics 5.0. The particle filter used for the solution of the inverse problem, which is coupled to the forward problem solution, was coded in Matlab* on an Intel(R) Xeon E56445@2.40 GHz dual processor with 32 GB of RAM memory.

4. Results and discussions

A 3D parallelepiped with dimensions $L_x = 80 \, \text{mm}$, $L_y = 40 \, \text{mm}$, and $L_z = 40 \, \text{mm}$ was considered for the analysis, with the tumor assumed as a sphere of radius 10 mm, located at the center of the parallelepiped. Both electrodes were considered as a square of 20 mm of side, so that $\Omega'_1 = \{-10 \text{ mm} \le$ $x \le 10 \text{ mm}, y = 20 \text{ mm}, 10 \text{ mm} \le z \le 10 \text{ mm}$ and $\Omega'_2 = \{-10 \text{ mm} \le x \le 10 \text{ mm}, y = -20 \text{ mm}, -10 \text{ mm} \le x \le 10 \text{ mm} \}$ mm < z < 10 mm} where the x, y, and z axes are supposed to be located at the tumor center (see Figure 1).

The healthy tissue is assumed as muscle. Thermophysical properties of healthy, blood, and tumor tissues are presented by Table 2. The initial condition for the bioheat transfer problem is the solution of the steady-state problem given by equations (18) to (20) with electrical heat source null, that is, $Q_e = 0$. For the convective boundary conditions, we assume $T_f = 20$ °C, $h_f = 45 \text{ W/m}^2\text{K}$ and the blood temperature as $T_b = 37$ °C [30]. The initial temperature field is presented by Figure 2.

Table 2. Properties of tissues.

Parameter	Healthy Tissue	Tumor	Blood
Thermal Conductivity (W/mK)	0.5	0.75	_
Specific Heat (J/kgK)	4200	4200	4200
Density (kg/m³)	1000	1000	1000
Perfusion Coefficient (s ⁻¹)	0.0005	0.002	_
Metabolic Heat Source (W/m³)	4200	42000	_

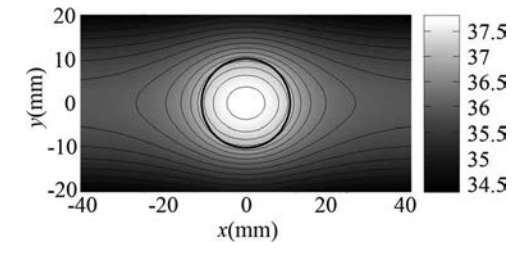


Figure 2. Initial temperature.



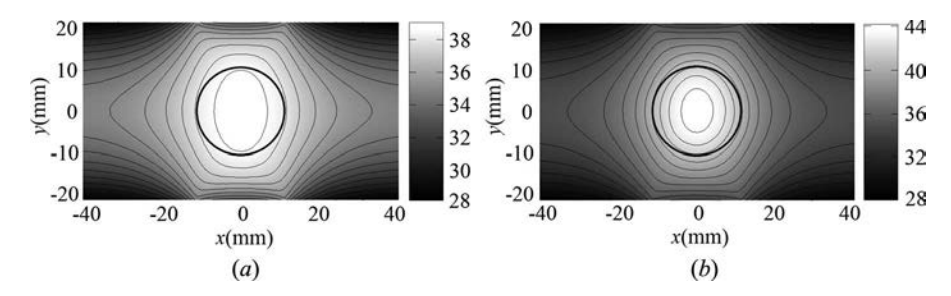


Figure 3. Exact temperature field at section z = 0 and t = 900 s: (a) without nanoparticles (b) with nanoparticles.

For the iron oxide nanoparticles (Fe₃O₄), the following parameters have been considered: thermal conductivity $k_3 = 40 \text{ W/mK}$, specific heat $c_{p3} = 4000 \text{ J/kgK}$, density $\rho_3 = 5180 \text{ kg/m}^3 [31]$; the properties for the tumor embedded with nanoparticles were given in terms of the rule of mixtures [36].

Heating was supposed to be imposed with a frequency f = 1 MHz. The electrical properties in the biological healthy tissue were $\sigma_1 = 0.50268$ S/m and $\epsilon_1 = 1836.4$ [62], while for the tumor tissue we have $\sigma_2' = 1.2\sigma_1$ and $\epsilon_2' = \epsilon_2 = 1.2\epsilon_1$ [30]. The electrical properties of the iron oxide nanoparticles were taken as $\sigma_3 = 25000$ S/m and $\chi'' = 18$ [31]. For all cases examined below, the number of nanoparticles was $n = 10^{14}$ with radius $r = 10^{-8}$ m, and the voltage at the electrode at the top boundary was U = 15 V, applied during 900 s. Figure 3a and b presents the exact temperature fields at t = 900 s over the surface z = 0, without and with nanoparticles loaded into the tumor, respectively. The analysis of these figures shows that the use of nanoparticles in the tumor locally increases the temperature in the region. While the maximum temperature without nanoparticles was 39.9°C, which is a low value for the hyperthermia treatment, the maximum temperature with nanoparticles was 44.25°C inside the tumor region, while the other regions were not thermally affected and still maintained low temperatures levels.

For the solution of the parameter and state estimation problem, temperature measurements of one single sensor were assumed available, located at the position $\{x = 0 \text{ mm}, y = 0 \text{ mm}, z = 0 \text{ mm}\}$. The measurements were generated from the solution of the direct (forward) problem with the parameters specified earlier. To avoid an inverse crime, the measurements were generated with 37856 elements in the region, while the inverse problem was solved with 16966 elements. Uncorrelated Gaussian errors with zero mean and standard deviation of 1°C were then added to the solution of the direct problem and the simulated measurements were supposed available every 20 s, during 900 s. Gaussian uncorrelated noise with zero mean and a standard deviation of 1°C was also added to the solution of the bioheat transfer problem, which served as the evolution model for the temperatures inside the domain and was solved with each sample of the Gaussian distribution of the electrical heat source. The evolution model for the electric field was taken as

$$\mathbf{E}_{k}^{i}(x, y, z) = \mathbf{E}_{k-1}^{i}(x, y, z) + \xi_{k}^{i}(x, y, z)$$
 (21)

where $\xi_k^i(x,y,z)$ is a Gaussian random vector with zero mean and standard deviation of 10% of the deterministic solution of the problem given by equations (10)–(13). The subscript k in equation (21) does not represent a time evolution of E(x,y,z), but the fact that it is treated as state variable for the application of the particle filter, which aims at the estimation of the electric heat source and of the transient temperature field, at the position (x,y,z) that corresponds to each finite element used for the numerical solution of the coupled electric and bioheat transfer problem. The particles $\mathbf{E}_0^i(x,y,z)$ at each position (x,y,z) were initially sampled from Gaussian distributions with means obtained from the deterministic solution of the electric problem and with standard deviations of 10% of these means.

Table 3. RMS errors.

Number of Particles	Mean (°C)	Standard Deviation (°C)	CPU time (h)
50	0.959	0.387	17.2
100	0.834	0.276	38.4
250	0.743	0.202	98.5

The prior probability densities for the model parameters θ were assumed as Gaussian, with zero mean and standard deviation of 10% of the mean value of each parameter. The vector of model parameters is given by

$$\mathbf{\theta} = [k_1, k_2, c_{p,b}, c_{p,1}, c_{p,2}, \rho_b, \rho_1, \rho_2, \omega_{b,1}, \omega_{b,2}, Q_{m,1}, Q_{m,2}, h_f, \sigma_1, \sigma_2, n, r, \chi'', R]$$
(22)

The effects of the number of particles on the estimation of parameters and state variables were examined by using 50, 100, and 250 particles. The accuracy of the estimation of state variables was addressed in terms of the means and standard deviations of the root mean square error, obtained with 10 repetitions of Liu and West's algorithm. The root mean square (RMS) error is given by

$$RMS = \sqrt{\frac{\sum\limits_{m=1}^{M} \left(T_{est,m} - T_{exa,m}\right)^2}{M}}$$
 (23)

where T_{est} represents the estimated values, T_{exa} represents the exact values, and M is the total number of elements and time steps.

Table 3 shows the means and standard deviations of the RMS errors for temperature. It is observed that the means and standard deviations of the RMS error decrease when the number of particles is increased, as expected. Figure 4 shows the estimated temperature field at the plane $z = 0 \,\mathrm{mm}$ and t = 900 s; the estimated maximum temperature in the region obtained with 50 particles was 43.81°C [Figure 4(a)], while it was 44.54°C with 100 particles [Figure 4(b)] and 44.27°C with 250 particles [Figure 4(c)]. The agreement between the maximum temperature estimated with 250 particles and the exact value of 44.25°C is excellent. A comparison of Figures 3b and 4 shows that all the estimated temperature fields are in quite good agreement with the exact one, but the estimations are

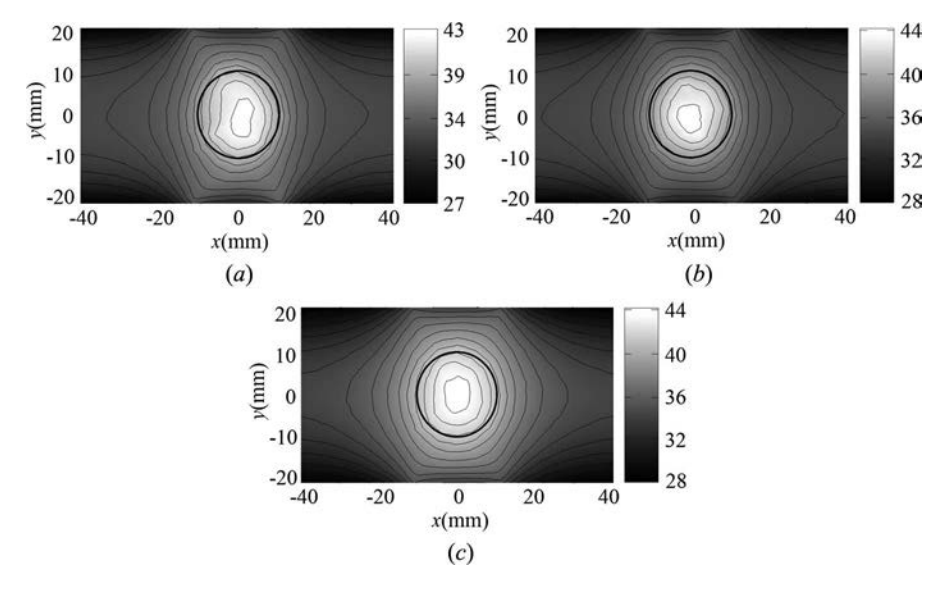


Figure 4. Estimated temperature field at section z = 0: (a) 50 particles, (b) 100 particles, (c) 250 particles.

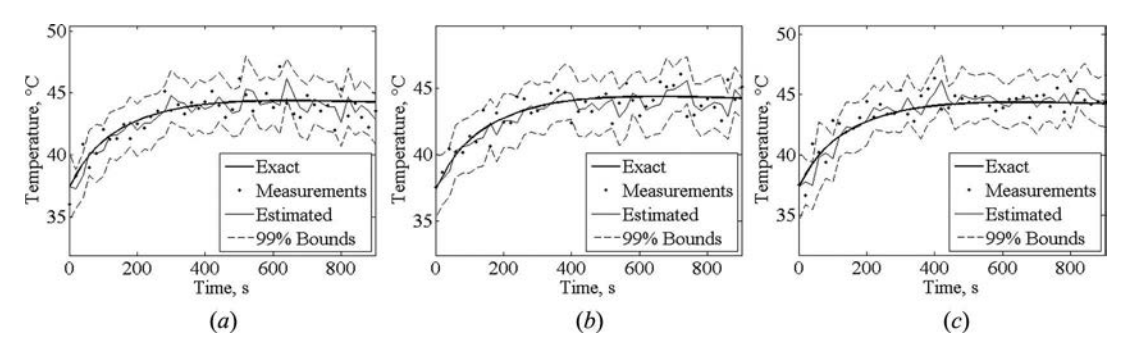


Figure 5. Estimated transient temperature at the sensor position (0,0,0): (a) 50 particles, (b) 100 particles, (c) 250 particles.

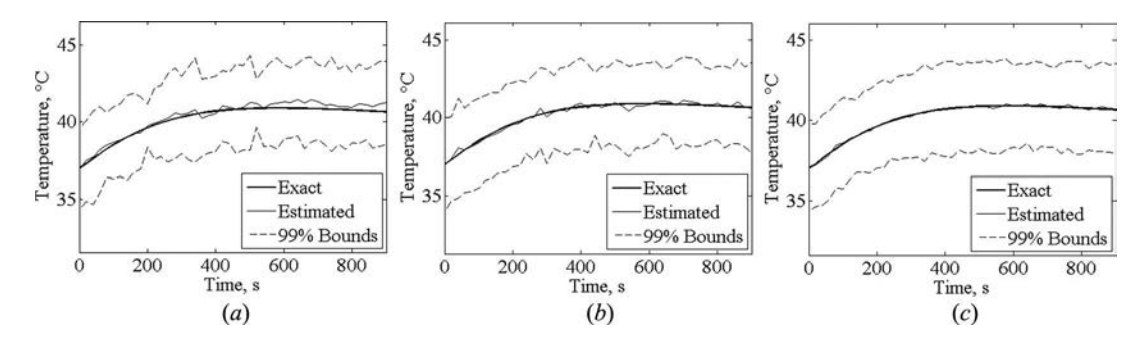


Figure 6. Estimated transient temperature at position (10,0,0) mm: (a) 50 particles, (b) 100 particles, (c) 250 particles.

smoother when the number of particles is increased, which is also evidenced by the reduction in the means and standard deviations of the RMS errors (see Table 3).

Figures 5 and 6 respectively present the estimated transient temperatures at the sensor position (0,0,0) mm and at the position (10,0,0) mm where no measurements are available, obtained with different number of particles. The 99% credible intervals are also presented in these figures. Figure 5 clearly shows that the estimated temperatures are more accurate than the available measurements. The

Table 4. Estimated mean values for the parameters.

		Estimated Mean Value			
Parameter	Exact Value	50 particles	100 particles	250 particles	
<i>k</i> ₁[W/mK]	0.5	0.43	0.46	0.47	
k_2 [W/mK]	0.75	0.67	0.72	0.78	
$\rho_1[kg/m^3]$	1000	1107.3	902	1021.5	
$\rho_2[kg/m^3]$	1000	950.6	1056.2	1028.3	
$\rho_b[kg/m^3]$	1000	958.85	1056	978.14	
$c_{p,1}$ [J/kgK]	4200	4227.3	4083	4179.5	
$c_{p,2}[J/kgK]$	4200	4142.9	4191.5	4197.1	
$c_{p,b}[J/kgK]$	4200	4659.9	4591.2	4328.3	
$\omega_{b,1}[s^{-1}]$	0.0005	0.00049	0.00047	0.00048	
$\omega_{b,2}[s^{-1}]$	0.002	0.0019	0.0022	0.0021	
$Q_{m,1}[W/m^3]$	4200	4557.6	4346	4189.7	
$Q_{m,2}[W/m^3]$	42000	44589.9	43962	42847.3	
$\sigma_1[S/m]$	0.50268	0.51076	0.54089	0.50806	
$\sigma_2[S/m]$	0.60322	0.62761	0.59137	0.60499	
$\chi^{''}$	18	15.88	17.01	18.48	
N	1×10^{14}	1.05600×10^{14}	1.06883×10^{14}	0.99271×10^{14}	
<i>r</i> [m]	1×10^{-8}	0.90034×10^{-8}	0.98641×10^{-8}	1.13359×10^{-8}	
R[mm]	10	9.8	10.4	10.2	
h_f [W/kgm ²]	45	41.8	42.19	44.9	

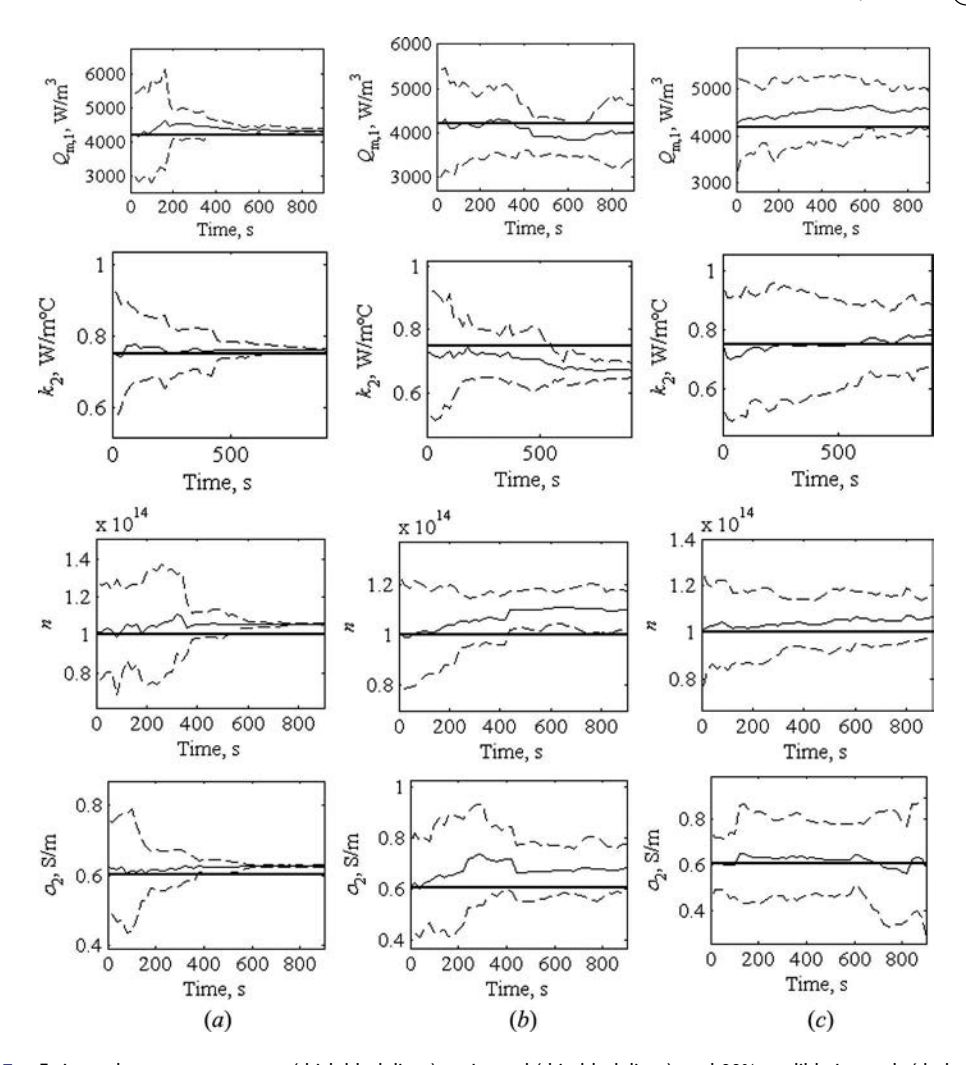


Figure 7. Estimated parameters – exact (thick black lines), estimated (thin black lines), and 99% credible intervals (dashed lines): (a) 50 particles, (b) 100 particles, (c) 250 particles.

agreement between estimated and exact temperatures is excellent also for the position where no measurements are available, as depicted from Figure 6. Both Figures 5 and 6 show that accurate means were estimated even with a small number of particles, such as 50. On the other hand, these figures show that the 99% credible intervals became smoother when the number of particles was increased.

Table 4 presents the mean values estimated for the parameters. Note that the estimated means are in excellent agreement with the exact ones, even with only 50 particles. Figure 7 shows the evolution in time of selected parameters and their 99% credible intervals. Despite the larger uncertainties in the measurements and in the evolution/observation models, the uncertainties related to the estimated parameters tend to decrease as time evolves and more information becomes available for the solution of the inverse problem. Indeed, the results presented earlier show that both parameters and state variables could be accurately recovered with Liu and West's algorithm of the particle filter.

5. Conclusions

The particle filter for combined parameter and state estimation was applied in this paper for a problem involving the radiofrequency hyperthermia treatment of cancer. The tumor was assumed as a



sphere loaded with iron oxide nanoparticles (F₃O₄) and surrounded by a healthy tissue. Uncertainties in the evolution model, temperature measurements, and model parameters were considered for the solution. The results obtained reveal that the algorithm of Liu and West is capable of providing accurate estimations for parameters and state variables, even for large uncertainties and a small number of particles. The estimated state variables and parameters were smoother and exhibited smaller variabilities as the number of particles was increased. Therefore, the approach implemented in this work has potential application in the planning and control of the hyperthermia treatment of cancer.

Funding

The financial support provided by FAPERJ, CAPES, and CNPq, Brazilian agencies for the fostering of science, is greatly appreciated. The authors also acknowledge the support provided by the STIC AmSud project "I3PE - Inverse Problems in Physical Properties Estimation."

References

- [1] P. Maybeck, Stochastic Models, Estimation and Control, NY, USA, 1979.
- [2] J. P. Kaipio and E. Somersalo, Computational and Statistical Methods for Inverse Problems, Springer, Berlin, Heidelberg, 2004.
- [3] J. M. Hammersley and D. C. Hanscomb, Monte Carlo Methods, Chapman & Hall, London, 1964.
- [4] R. Winkler, An Introduction to Bayesian Inference and Decision, Probabilistic Publishing, Gainsville, Florida,
- [5] N. Gordon, D. Salmond, and A. F. M. Smith, Novel Approach to Nonlinear and Non-Gaussian Bayesian state estimation, Proc. Inst. Elect. Eng., vol. 140, pp. 107-113, 1993.
- [6] M. K. Pitt and N. Shephard, Filtering via Simulation: Auxiliary Particle Filters, J. Am. Stat. Assoc., vol. 94, pp. 1–41,
- [7] J. Liu and M. West Combined Parameter and State Estimation In Simulation Based Filtering, in: S. A. Doucet, N. de Freitas, and N. Gordon (eds.), Seq. Monte Carlo Methods Pract., New York, 2001, pp. 197-217.
- [8] M. West, Approximating Posterior Distributions by Mixture, J. R. Stat. Soc. B. vol. 55, pp. 409-422, 1993.
- [9] M. M. Saito, S. Imoto, R. Yamaguchi, H. Sato, H. Nakada, M. Kami, et al., Extension and Verification of the SEIR Model on the 2009 Influenza A (H1N1) Pandemic in Japan, Math. Biosci., vol. 246, pp. 47-54, 2013.
- [10] A. Skvortsov and B. Ristic, Monitoring and Prediction of an Epidemic Outbreak Using Syndromic Observations, Math. Biosci., vol. 240, pp. 12-19, 2012.
- [11] L.-J. Kao, An Application of a Two-level Non-Gaussian State-space Model in the Analysis of Longitudinal Papilloma Count Data, Math. Biosci., vol. 199, pp. 121-140, 2006.
- [12] J. M. J. Costa, H. R. B. Orlande, H. F. Campos Velho, S. T. R. Pinho, G. S. Dulikravich, R. M. Cotta, and S. Cunha, Estimation of Tumor Size Evolution Using Particle Filters, J. Comput. Biol., vol. 22, pp. 1–17, 2015.
- [13] D. M. Sheinson, J. Niemi, and W. Meiring, Comparison of the Performance of Particle Filter Algorithms Applied to Tracking of a Disease Epidemic, Math. Biosci., vol. 255C, pp. 21-32, 2014.
- [14] W. Y. Tan and Z. Ye, Estimation of HIV Infection and Incubation via State Space Models, Math. Biosci., vol. 167, pp. 31-50, 2000.
- [15] L. A. Bermeo Varon, H. R. B. Orlande, and G. Elicabe, Estimation of state variables in the hyperthermia therapy of cancer with heating imposed by radiofrequency electromagnetic waves, Int. J. Therm. Sci., vol. 98, pp. 228-236,
- [16] B. Lamien, H. R. B. Orlande, G. E. Elicabe, and A. J. Maurente, State Estimation Problem in Hyperthermia Treatment of Tumors Loaded with Nanoparticles, in: Proc. 15th Int. Heat Transf. Conf. IHTC-15, Kyoto, Japan, 2014.
- [17] P. Cherukuri, E. S. Glazer, and S. A. Curley, Targeted hyperthermia using metal nanoparticles, Adv. Drug Deliv. Rev., vol. 62, pp. 339-45, 2010.
- [18] E. Majchrzak and M. Paruch, Numerical Modelling of Temperature Field in the Tissue with a Tumor Subject to the Action of Two External Electrode, Sci. Res. Inst. Math. Comput. Sci., vol. 1, pp. 1-8, 2009.
- [19] E. Majchrzak and M. Paruch, Numerical Modelling of Tissue Heating by Means of the Electromagnetic Field, Sci. Res. Inst. Math. Comput. Sci., vol. 9, pp. 89-97, 2010.
- [20] E. Kurgan and P. Gas, Estimation of Temperature Distribution Inside Tissues in External RF Hyperthermia, Prz. Elektrotechniczny., vol. 86, pp. 100-102, 2010.
- [21] E. Kurgan and P. Gas, Treatment of Tumors Located in the Human Thigh using RF Hyperthermia, Prz. Elektrotechniczny., vol. 87, pp. 103-106, 2011.
- [22] M. Jamil and E. Y. K. Ng, To Optimize the Efficacy of Bioheat Transfer in Capacitive Hyperthermia: A Physical Perspective, J. Therm. Biol., vol. 38, pp. 272-279, 2013.



- [23] E. Y. K. Ng and M. Jamil, Parametric Sensitivity Analysis of Radiofrequency Ablation with Efficient Experimental Design, Int. J. Therm. Sci., vol. 80, pp. 41-47, 2014.
- [24] M. Jamil and E. Y. K. Ng, Statistical Modeling of Electrode based Thermal Therapy with Taguchi based Multiple Regression, Int. J. Therm. Sci., vol. 71, pp. 283-291, 2013.
- [25] L. A. Dombrovsky, J. Randrianalisoa, W. Lipinski, and V. Timchenko, Simplified Approaches To Radiative Transfer Simulations in Laser-Induced Hyperthermia of Superficial Tumors, Comput. Therm. Sci., vol. 5, pp. 521-530, 2013.
- [26] L. A. Dombrovsky, V. Timchenko, and M. Jackson, Indirect Heating Strategy for Laser Induced Hyperthermia: An Advanced Thermal Model, Int. J. Heat Mass Transf., vol. 55, pp. 4688-4700, 2012.
- [27] L. A. Dombrovsky, V. Timchenko, C. Pathak, H. Piazena, W. Müller, and M. Jackson, Radiative Heating of Superficial Human Tissues with the Use of Water-Filtered Infrared-A Radiation: A Computational Modeling, Int. J. Heat Mass Transf., vol. 85, pp. 311-320, 2015.
- [28] M. R. Horsman and J. Overgaard, Hyperthermia: a potent enhancer of radiotherapy, Clin. Oncol. (R. Coll. Radiol), vol. 19, pp. 418-26, 2007.
- [29] R. Colombo, L. F. Da Pozzo, A. Salonia, P. Rigatti, Z. Leib, J. Baniel, et al., Multicentric Study Comparing Intravesical Chemotherapy Alone and With Local Microwave Hyperthermia for prophylaxis of recurrence of superficial transitional cell carcinoma, J. Clin. Oncol., vol. 21, pp. 4270-4276, 2003.
- [30] E. Majchrzak and M. Paruch, Numerical Modelling of the Cancer Destruction During Hyperthermia Treatment, Comput. Methods Mech., pp. 1-6, 2011.
- [31] Y.-G. Lv, Z.-S. Deng, and J. Liu, 3-D Numerical Study on the Induced Heating Effects of Embedded Micro/ Nanoparticles on Human Body Subject to External Medical Electromagnetic Field, IEEE Trans. Nanobioscience., vol. 4, pp. 284-294, 2005.
- [32] A. Miaskowski and B. Sawicki, Magnetic Fluid Hyperthermia Modeling Based on Phantom Measurements, and Realistic Breast Model, IEEE Trans. Biomed. Eng., vol. 60, pp. 1806-1813, 2013.
- [33] E. Majchrzak and M. Paruch, Identification of Electromagnetic Field Parameters Assuring the Cancer Destruction During Hyperthermia Treatment, Inverse Probl. Sci. Eng., vol. 19, pp. 45-58, 2011.
- [34] E. Kurgan and P. Gas, Simulation of the Electromagnetic Field And Temperature Distribution in Human Tissue in RF Hyperthermia, Prz. Elektrotechniczny., vol. 1, pp. 171-174, 2015.
- [35] M. Paruch, Hyperthermia Process Control Induced by the Electric Field in Order to Cancer Destroying, Acta Bioeng. Biomech., vol. 16, pp. 123-130, 2014.
- [36] W. Andra, C. G. Ambly, R. Hergt, I. Hilger, and W. A. Kaiser, Temperature Distribution as Function of Time Around a Small Spherical Heat Source of Local Magnetic Hyperthermia, J. Magn. Magn. Mater., vol. 194, pp. 197-203, 1999.
- [37] T. O. Tasci, I. Vargel, A. Arat, E. Guzel, P. Korkusuz, and E. Atalar, Focused RF Hyperthermia Using Magnetic Fluids, Med Phys., vol. 36, pp. 1906–1912, 2009.
- [38] M. T. Basel, S. Balivada, H. Wang, T. B. Shrestha, G. M. Seo, M. Pyle, et al., Cell-delivered Magnetic Nanoparticles Caused Hyperthermia-Mediated Increased Survival in a Murine Pancreatic Cancer Model, Int. J. Nanomedicine., vol. 7, pp. 297–306, 2012.
- [39] R. Hergt, S. Dutz, R. Müller, and M. Zeisberger, Magnetic Particle Hyperthermia: Nanoparticle Magnetism and Materials Development for Cancer Therapy, J. Phys. Condens. Matter., vol. 18, pp. S2919–S2934, 2006.
- [40] K. Murase, J. Oonoki, H. Takata, R. Song, A. Angraini, P. Ausanai, et al., Simulation and Experimental Studies on Magnetic Hyperthermia with use of Superparamagnetic Iron Oxide Nanoparticles, Radiol. Phys. Technol., vol. 4, pp. 194-202, 2011.
- [41] L. A. Dombrovsky, V. Timchenko, M. Jackson, and G. H. Yeoh, A Combined Transient Thermal Model for Laser Hyperthermia of Tumors with Embedded Gold Nanoshells, Int. J. Heat Mass Transf., vol. 54, pp. 5459-5469, 2011.
- [42] S. Eibner, R. Alfredo, O. Jaime, B. Lamien, R. Basto, H. Orlande, and O. Fudym, Near Infrared Light Heating of Soft Tissue Phantoms Containing Nanoparticles, Thermal Engineering., vol. 13, pp. 13–18, 2014.
- [43] L. A. Dombrovsky, V. Timchenko, and M. Jackson, Indirect Heating Strategy for Laser Induced Hyperthermia: An Advanced Thermal Model, Int. J. Heat Mass Transf., vol. 55, pp. 4688-4700, 2012.
- [44] Y. Bayazitoglu, Nanoshell Assisted Cancer Thermal Therapy: Numerical Simulations, in: Proc. ASME 2009 2nd Int. Conf. Micro/Nanoscale Heat Mass Transf. Int. Conf., Shanghai, China, pp. 545-552, 2009.
- [45] X. Xu, A. Meade, and Y. Bayazitoglu, Numerical Investigation of Nanoparticle-assisted Laser-induced Interstitial Thermotherapy Toward Tumor and Cancer Treatments, Lasers Med Sci., vol. 26, pp. 213–222, 2011.
- [46] X. Xu, A. Meade, and Y. Bayazitoglu, Feasibility of Selective Nanoparticle-assisted Photothermal Treatment for an Embedded Liver Tumor, Lasers Med Sci., pp. 1-10, 2012.
- [47] Y. Zhang, B. Chen, D. Li, and G. Wang, Efficient and Accurate Simulation of Light Propagation in Bio-tissues Using the Three-dimensional Geometric Monte Carlo method, Num. Heat Transfer - Part A, vol. 68, pp. 827–846, 2015.
- [48] I. Im, S. Yun, and K. Kim, Numerical Study on the Temperature Profiles and Degree of Burns in Huma Skin Tissue Combined Thermal Therapy, Num Heat Transfer - Part A, vol. 67, pp. 921-933, 2015.



- [49] A. AlAmiri, K. Khanafer, and K. Vafai, Flui-structure Interactions in Tissue During Hyperthermia, Num Heat Transfer - Part A, vol. 66, pp. 1-16, 2014.
- [50] T. Wu, P. Li, Q. shao, J. Hong, L. Yang, and S. Wu, A Simulation-Experiment Method to Chracterize the Heat Transfer in Ex-vivo Porcine Hepatic Tissue with Realistic Microwave Ablation System, Num Heat Transfer - Part A, vol. 64, pp. 729–743, 2013.
- [51] N. Afrin, J. Zhou, D. Tzou, and J. chen, Numerical Simulation of Thermal Damage of Living Biological Tissues Induced by Laser Irradiation Based on the Generalized Dual Phase Lag Model, Num Heat Transfer - Part A, vol. 61, pp. 483-501, 2012.
- [52] M. S. Arulampalam, S. Maskell, N. Gordon, T. Clapp, A Tutorial on Particle Filters for Online Nonlinear/ non-Gaussian Bayesian Tracking, IEEE Trans. Signal Process., vol. 50, pp. 174-188, 2002.
- [53] B. Ristic, M. S. Arulampalam, and N. Gordon, Beyond the Kalman Filter, Artech House, Boston, MA, 2004.
- [54] C. Andrieu, A. Doucet, and C. P. Robert, Computational Advances for and from Bayesian, Analysis, Stat. Sci., vol. 19, pp. 118–127, 2004.
- [55] P. Wust, B. Hildebrandt, G. Sreenivasa, B. Rau, J. Gellermann, H. Riess, et al., Review Hyperthermia in Combined Treatment of Cancer, Lancet Oncol., vol. 3, pp. 487-497, 2002.
- [56] C. K. Chou and R. Ren Radio Frequency Hyperthermia in Cancer Therapy, in: Biomed. Eng. Handb., 2nd ed., 2000.
- [57] H. H. Pennes, Analysis of Tissue and Arterial Blood Temperatures in the Resting Human Forearm, J. Appl. Physiol., vol. 1, pp. 93-124, 1948.
- [58] R. Turner and M. Streicher, Measuring Temperature using MRI: A Powerful and Versatile Technique, Magn Reson Mater Phy., vol. 25, pp. 1-3, 2012.
- [59] D. K. Cheng, Fundamentals of Engineering Electromagnetics, Addison-Wesley Publishing Company, Inc, USA,
- [60] R. E. Rosensweig, Heating Magnetic Fluid with Alternating Magnetic Field, J. Magn. Magn. Mater., vol. 252, pp. 370-374, 2002.
- [61] Q. A. Pankhurst, J. Connolly, S. K. Jones, and J. Dobson, Applications of Magnetic Nanoparticles in Biomedicine, J. Phys. D. Appl. Phys., vol. 36, pp. R167-R181, 2003.
- [62] S. Gabriel, R. W. Lau, and C. Gabriel, The Dielectric Properties of Biological Tissues: III. Parametric Models for the Dielectric Spectrum of Tissues, Phys. Med. Biol., vol. 41, 2271-2293, 1996.